Succinct Papers

Signal and Noise Analysis of a Loop-Monopole Active Antenna

WILLIAM C. WONG

Abstract—Directional active antennas have been widely studied over the past decade. Most of the efforts have been experimental rather than analytical. The experimental work of Meinke led to the development of an electrically small loop-monopole active antenna suitable for direction finding. This paper shows that performance characteristics such as the noise figures and radiation patterns of the active loop-monopole antenna can be analytically predicted. The analytical techniques used involved the integral equation solutions by the moments method together with standard RF circuit analysis. The predicted results agreed quite well with measurements. Although the antenna is electrically small, any attempt to predict the antenna performance using only the circuit approach may not work, as the mutual coupling between the loop and monopole has a strong effect on both the signal and the noise.

Paper received November 10, 1973; revised January 16, 1974. This work was supported by the Air Force Avionics Laboratory, Air Force Systems Command, Wright-Patterson AFB, Ohio, under Contract F33615-71-C-1285.

The author is with the Radio Frequency Laboratory, TRW Systems Group, Redondo Beach, Calif. 90278.

I. INTRODUCTION

Directional active antennas have been studied extensively by Meinke [1]–[3]. Among the numerous receive-only antenna configurations he investigated was the loop-monopole configuration shown in Fig. 1. Despite its small size (fraction of a wavelength), the loop-monopole is capable of a directivity suitable for such applications as a direction-finder (DF) antenna. This particular configuration is rigorously treated in this paper by solving the integral equation for the antenna currents simultaneously with the algebraic equations describing the two-port containing Van der Ziel noise

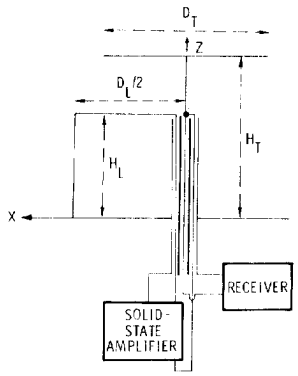

(a)

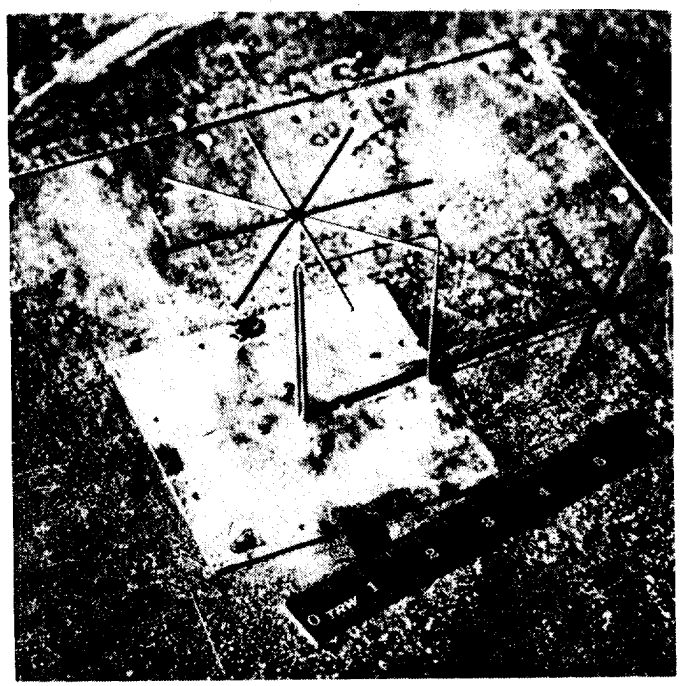

(b)

Fig. 1. Loop-monopole solid-state antenna. Three coax cables are bounded so that outer conductors are in good electrical contact.

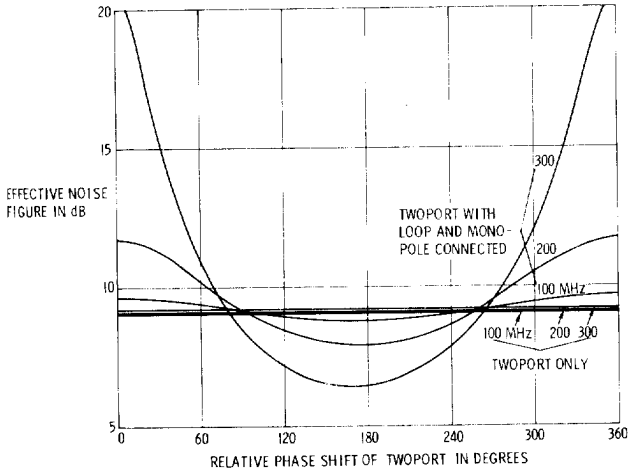

Fig. 2. Effective noise figure versus relative phase shift of two-port at different frequencies for two-port only and two-port with loop and monopole connected.

generators in transistors and Nyquist generators for resistors. This complete model is necessary because any attempt to predict the antenna performance characteristics such as the noise temperature without considering the mutual coupling between the loop and monopole may not work as evidenced by Fig. 2, which shows that the noise temperature of an active antenna is sensitive to the phase shift of the amplifier, but that of the amplifier is relatively independent of the phase shift.

In Meinke's original configuration, the amplifier was mounted at the tap point on the monopole. In an attempt to make the structure more rugged, the amplifier was mounted under the ground plane and it was connected to the tap point by means of coax cables. The effect of the coax on the performance characteristics of the antenna is discussed. With the amplifier mounted under the ground plane, the resulting structure is still an active antenna because the amplifier is still an integral part of the antenna and it is used to control the signal from the loop before combining with the signal from the monopole.

Two parameters of interest will be treated in this paper, namely, the signal and the noise. The signal is defined in this paper as the mean-square output voltage when the incident field polarized in the direction parallel to the monopole is of unity intensity. The output noise of the antenna is a linear sum of the internal noise and the amplified external noise. The amplified external noise depends on the environment in which the antenna is operated and constitutes a minimum noise that must be accepted. Internal noise constitutes an additional noise that degrades the system. In this analysis, only the internal noise will be considered. Moreover, the internal noise is restricted to the thermal noise produced in resistive components and the shot noise generated at transistor junctions. Negative feedback is used in the amplifier to minimize nonlinearity, so that the effects of cross-modulation and intermodulation are assumed negligible.

No attempt was made to design the amplifier so as to achieve optimum antenna performance. In fact, the voltage gain of the amplifier used to demonstrate the correctness of the analysis was arbitrarily chosen to be unity. Questions regarding the efficiency and the relative performance of the active loop-monopole antenna to a passive loop-monopole antenna will be dealt with in a future paper, since the purpose of this paper is to present a signal-to-noise analysis of active antennas in general and then to apply it to the loop-monopole antenna as an example.

II. EXPRESSIONS FOR SIGNAL AND NOISE

Inasmuch as the loop and monopole are electrically close to each other, electromagnetic interaction exists between them. To account for this coupling between the input and output ports of the amplifier, circuit equations and the electromagnetic field equations must be solved simultaneously. The active antenna can be thought of as having an equivalent circuit shown in Fig. 3, in which the two-port contains the input and output transmission lines and a single stage transistor amplifier. In practice, the output terminal of the antenna is connected through a transmission line to a matched receiver. In this analysis, the transmission line/receiver combination is replaced by the characteristic impedance of the line Z_0 and is treated as a part of the two-port. As far as the wire structure is concerned, the two-port is infinitesimal in size, thus making it possible to relate the two-port terminal voltages to the tangential E-field in the neighborhood of the tap point.

Since both the antenna and the two-port are linear, the output power is a linear combination of the signal due to the excitation of the antenna by an incident plane wave and the noise due to the excitation of the antenna by the noise generators within the two-port. The signal and noise can, therefore, be evaluated independently.

A. Expression for Signal

To obtain the output signal, the two-port is assumed to be noise free, so that its terminal voltages $\bar{V}$ are related to the terminal currents $\bar{I}$ by the impedance matrix $\bar{\bar{Z}}$ as follows:

$$\bar{V} = \bar{\bar{Z}} \cdot \bar{I}. \tag{1}$$

The antenna is assumed to be excited by a plane wave of unity intensity polarized along the axis of the monopole

$$\bar{E}_i = \hat{u}_Z \exp(-j\bar{k} \cdot \bar{r}). \tag{2}$$

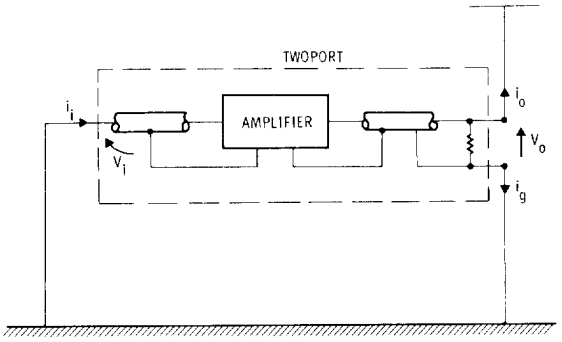

Fig. 3. Antenna equivalent circuit.

The incident field induces on the antenna a current $\bar{J}$ that gives rise to the scattered field

$$\bar{E}_s(\bar{r}) = \bar{E}_t(\bar{r}) - \bar{E}_i(\bar{r}) = \int \bar{\bar{\Gamma}}(\bar{r},\bar{r}') \cdot \bar{J}(\bar{r}')\, dr' \tag{3}$$

where $\bar{E}_s$ is the scattered field due to the induced current $\bar{J}$, $\bar{E}_t$ is the total field, $\bar{E}_i$ is the incident field, $\bar{\bar{\Gamma}}$ is the free-space tensor Green's function, and the line integral is taken over the entire wire structure of the mathematical model shown in Fig. 3 in which the ground plane is replaced by the image of the antenna above the ground plane.

The boundary conditions are that the total $\bar{E}$ field everywhere along the wire structure is related to the current on the wire by Ohm's law and that it is related to the two-port terminal voltages at the tap point. The integral equation together with the boundary conditions are then approximated by a set of linear equations using the method of moments [6], [7]. This set of equations and the set describing the two-port given by (1) are solved simultaneously to yield

$$\bar{v} = \bar{\bar{\gamma}} \cdot \bar{C} \tag{4}$$

where $\bar{\bar{\gamma}}$ is a square matrix which is a function of the wire resistivity, the two-port parameters, and the self- and mutual-impedance terms for the subsections of the wire structure; $\bar{C}$ is a column matrix whose elements are the coefficients of the expansion functions approximating the currents on the wire; and $\bar{v}$ is a column matrix proportional to the incident field. Solving (4) yields the two-port terminal currents from which the output voltage of the two-port can be obtained from (1).

B. Expression for Noise

To obtain the output noise, the external excitation is removed and the amplifier is assumed to have a noise equivalent circuit as shown in Fig. 4. Each resistor within the amplifier has associated with it a Johnson noise generator. The transistor is characterized by two noise current generators to account for the shot noises generated at the emitter and collector junctions, respectively, and a noise voltage generator to account for the thermal noise of the base spreading resistance [4], [5]. Cross-correlation only exists between the two noise current generators within the transistor. No correlation exists between any other pair of noise generators within the two-port.

Let there be N noise generators within the two-port and let the amplifier be linear. Then it can be shown that the two-port can be characterized by [10]

$$\bar{V} = \bar{\bar{Z}} \cdot \bar{I} + \bar{\bar{U}} \cdot \bar{n} \tag{5}$$

where $\bar{V}$ and $\bar{I}$ are, respectively, the terminal voltage and current vectors so that $\bar{\bar{Z}}$ is the impedance matrix for the two port, $\bar{n}$ is an N-element noise vector representing the rms voltages and currents per cycle of the N noise generators within the two-port, and U is a linear operator that operates on the noise vector to give the effects of the noise sources on the terminal voltages of the two-port. Thus the antenna is essentially a transmitting antenna, excited by the noise generators within the two-port.

As before, the integral equation, together with the boundary conditions, is approximated by a set of linear equations which is

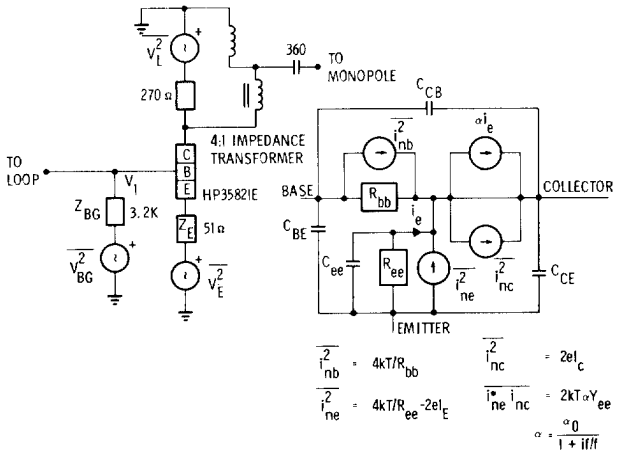

Fig. 4. Transistor noise equivalent circuit.

solved simultaneously with (5) to express the two-port terminal currents in terms of the noise vector (see Appendix I) as follows:

$$\bar{I} = \bar{\bar{\alpha}} \cdot \bar{\bar{U}} \cdot \bar{n}. \tag{6}$$

where $\bar{\bar{\alpha}}$ is a 2×2 matrix whose elements are functions of both the antenna and the two-port parameters.
Substituting (6) into (5) yields

$$\bar{V} = \bar{\bar{U}} \cdot \bar{n} + \bar{\bar{Z}} \cdot \bar{\bar{\alpha}} \cdot \bar{\bar{U}} \cdot \bar{n}. \tag{7}$$

The first term gives the noise generated terminal voltages of the two port in the absence of the antenna. With the loop and monopole connected, the noise generated terminal voltages are modified by an amount equal to the second term in (7).

Equation (7) can be put more succinctly in the form

$$\bar{V} = \bar{\bar{\mu}} \cdot \bar{n} \tag{8}$$

where $\bar{\bar{\mu}}$ is a $2 \times N$ matrix that operates on the N element noise vector $\bar{n}$ to give the two-port terminal voltages. Let the first pair of elements in the noise vector correspond to the correlated shot noise generators in the transistor. Then the two-port output mean-square noise voltage is given by

$$\overline{V_n^2} = \sum_{i=1}^{N} |\mu_{2i} n_i|^2 + 2 \operatorname{Re}\left[(\mu_{2,1}^* \mu_{2,2})\, \overline{(n_1^* n_2)}\right] \tag{9}$$

where the asterisk denotes complex conjugate and the bar denotes cross-correlation. The expression for the cross-correlation between the two shot noise generators within the same transistor is given in [4], [5], and [9].

Equation (4) will be used in conjunction with (1) to compute the antenna patterns and (9) will be used to obtain antenna noise figures.

Several procedures were employed to check the validity of the derived equations. One procedure used was the convergence test, in which the number of expansion functions used to approximate the current distribution on the wire was doubled and quadrupled, and the computed signal and noise in the three cases were found to be stationary. Another check procedure used was to examine the continuity of currents at the junction between the monopole and the top load. The current flowing into the node was found to be discontinuous from the currents flowing out of the node by an amount less than 2 per cent of the incident current. The slight discrepancy is probably due to the inherent numerical accuracy problem. The last check procedure was a comparison between calculated and measured results.

III. EXPERIMENTAL VERIFICATION OF ANTENNA PATTERNS

In the mathematical modeling of the antenna, the ground plane was replaced by the image of the antenna. In the experimental pattern measurements, the loop monopole was mounted on the

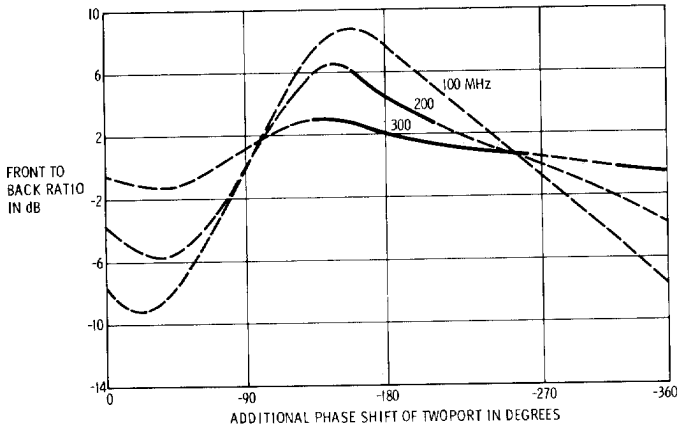

Fig. 5. Front-to-back characteristics for ideal two-port located at tap point.

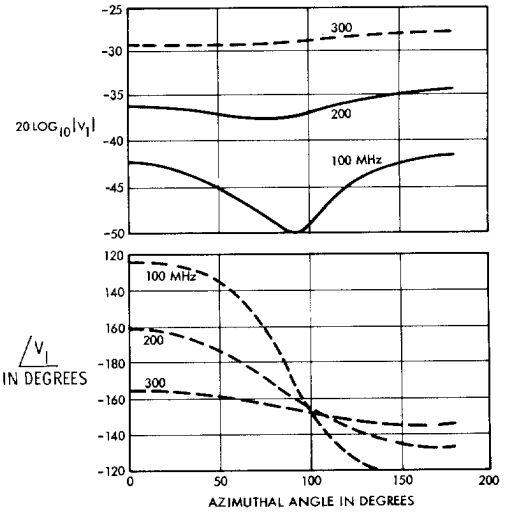

Fig. 6. Dependence of two-port input voltage upon angle of incidence.

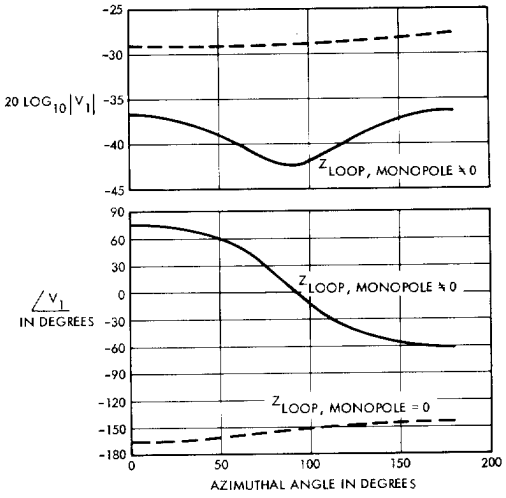

Fig. 7. Effect of mutual coupling between loop and monopole upon two-port input voltage.

ground plane consisting of a 24 ft × 24 ft 0.25 in wire mesh. The antenna under test had the following physical dimensions: D_T = 4 in, H_T = 4 in, D_L = 4 in, H_L = 3 in, where the symbols are defined in Fig. 1. Antenna pattern measurements at different frequencies were made from which the front-to-back ratios were obtained and compared with the theoretically predicted results. The front-to-back ratio is defined in this paper as 20 $\log_{10} | V_0(\phi = 180°)/V_0(\phi = 0°) |$, where V_0 is the amplifier output voltage, and ϕ is the angle between the direction of propagation of the incident wave and the x direction, which contains the loop driving the amplifier as shown in Fig. 1. It turns out that the phase shift of the two-port plays an important role in determining the noise as well as the character of the radiation pattern. To bring into perspective the dependence of the signal and noise on the phase shift, a phase shifter is introduced into the two-port. The phase of the phase shifter is varied, the resulting patterns are calculated, and the front-to-back ratios of these patterns are plotted against the phase of the phase shifter for frequencies of 100, 200, and 300 MHz.

Fig. 5 shows the front-to-back characteristics for the amplifier located at the tap point, Fig. 8 shows those for the amplifier under the ground plane, and Fig. 9 is the same as Fig. 8 except that included in the calculations were the measured strays of the actual amplifier with discrete components, which has a broad-band transmission line transformer for impedance matching.

In what follows, a figure eight pattern is defined as a pattern with two equal minima while a cardioid is a pattern with a single minimum. In Figs. 5, 8, and 9 the broken lines represent the regions over which the antenna has a figure eight pattern and the solid line is the region over which the pattern is a cardioid. Inspection of Fig. 5 shows that the particular amplifier arbitrarily chosen for experimental verification of the theory would make a poor DF antenna; at 100 MHz a cardioid pattern is not achievable, while at 200 and 300 MHz where it is possible to obtain a cardioid by proper phase control, the maximum achievable front-to-back ratio is only 6 dB and 3 dB, respectively. In an attempt to understand why the maximum achievable front-to-back ratio of the antenna under consideration diminishes with increasing frequency, the amplitude and phase of the voltage V_1 appearing at the input port of the two port is plotted in Fig. 6, which, shows that the greater the dependence of V_1 on the angle of incidence, the greater is the maximum achievable front-to-back ratio as shown in Fig. 5. The fact that the angular dependence of V_1 diminishes with increasing frequency is a clear indication that the mutual coupling between the loop and monopole is important. To demonstrate that this is indeed the case, Fig. 7 is included which shows the effect of the monopole on V_1. In the absence of mutual coupling, the variations of both the amplitude and phase of V_1 are much more pronounced: the presence of a dip rather than a null in $| V_1 |$ when the azimuth angle is 90° is due to the fact that the amplifier is not symmetrically located with respect to the loop. Thus while both the loop and the monopole are needed to produce a cardioid, the mutual coupling between them is a limiting factor on the antenna bandwidth.

Fig. 8 shows that the maximum achievable front-to-back ratio is appreciably improved by the introduction of a pair of transmission lines which enable the amplifier to be mounted under the ground plane. This improvement brought about by the transmission line is clearly fortuitous, but it does mean that the transmission line must also have changed the amplitude response of the two-port in addition to the phase response. This is because the input transmission line is not matched at the amplifier. Thus from Figs. 5 and 8 it is clear that both the amplitude and the phase responses of the amplifier play an important role in determining the character of the radiation pattern, as might be expected. Fig. 9 shows the plots corresponding to the actual antenna built with discrete components, which have considerable strays associated with them. The measured front-to-back ratios at 100, 200, and 300 MHz are shown, respectively, by the dot, tiangle, and cross. The agreement between the measured and calculated results is seen to be quite good. It should be mentioned that the measured pattern was a cardioid at 300 MHz and those at 100 and 200 MHz were a figure eight as predicted by calculations. The reader's attention is also drawn to the fact that a phase shift of a mere 10° at 200 MHz would bring the measured result in coincidence with the calculated result.

IV. EXPERIMENTAL VERIFICATION OF ANTENNA NOISE FIGURE

The antenna noise figure (NF) is defined as

$$\mathrm{NF} = 10 \log_{10}(1 + T_n°/297°\mathrm{K}) \tag{10}$$

where $T_n°$ is the noise temperature in degrees Kelvin of the active antenna. In terms of the mean square voltage $\overline{V_n^2}$ given by (9),

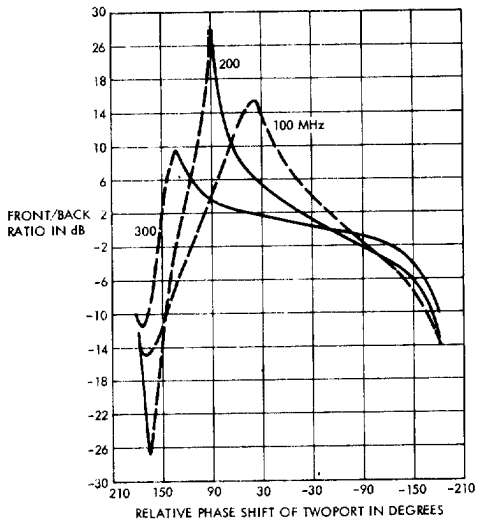

Fig. 8. Front-to-back characteristics for ideal two-port located under ground plane.

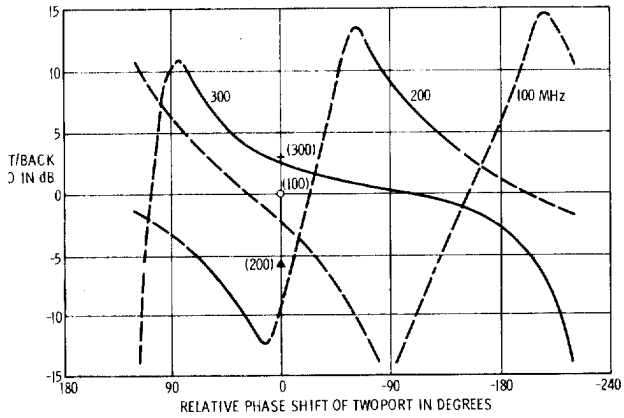

Fig. 9. Front-to-back characteristics for actual two-port located under ground plane.

the noise temperature is

$$T_u = \overline{V_n^2}/(kZ_0) \tag{11}$$

where k is the Boltzmann constant.

The calculated NF was obtained using (9) through (11), and the measured NF was obtained using (10), in which the noise temperature was measured with the standard Y-factor technique in a shielded chamber.

Both the calculated and measured noise figures for the antenna at 70 and 200 MHz, respectively, are tabulated in Table I.

The antenna noise in general should be higher at higher frequencies. The observed discrepancy is due to the fact that the actual amplifier has appreciable stray capacitance at its output terminal, which shunts a part of the noise to ground.

V. CONCLUSIONS

Expressions for the signal and noise of a loop monopole active antenna were derived. Validity of the signal and noise expressions was checked using the convergence test, the equation of continuity test, and experimental measurements of the front to back ratio and noise. All three procedures seem to bear out the correctness of the expressions. The electromagnetic approach to the problem is necessary, despite the fact that the antenna is electrically small, because the inclusion of the mutual coupling between the loop and monopole is essential in predicting both the signal and the noise of the antenna. In fact, the mutual coupling is a limiting factor for the bandwidth of the antenna. The ohmic loss in the wire was found to have a negligible effect on the signal and noise, probably due to the fact that its equivalent lumped resistance is small compared with the resistances associated with the amplifier.

TABLE I
CALCULATED AND MEASURED NOISE FIGURES

Frequency	Calculated	Measured
70 MHz	8.7 dB	9.2 dB
200 MHz	7.22 dB	7.5 dB

APPENDIX I
DETERMINATION OF SIGNAL AND NOISE OF LOOP-MONOPOLE ANTENNAFIER

To solve the integral equation given by (3) we let the current be expressed in terms of a set of N_a sinusoidal expansion functions f_n, as follows:

$$\bar{J}(\bar{r}') = \sum_{n=1}^{N_a} \hat{u}_n C_n f_n(\bar{r}') \tag{I-1}$$

with

$$f_n(\bar{r}) = \sin k\left(\frac{L_n}{2} - |s|\right) \tag{I-2}$$

where $\hat{u}_n$ is the unit vector of the nth current element, C_n is the unknown coefficient associated with the nth current element, k is the free-space wavenumber, L_n is the length of the nth dipole, and s is the distance along the nth element measured from the center of the dipole.

Using the method of moments [6], [7], the integral equation can be approximated by the set of linear equations,

$$\int_{L_m} ds\, f_m(\bar{r})\,\hat{u}_m \cdot \bar{E}_t(\bar{r}) - V_{im} = \sum_{n=1}^{N_a} \beta_{mn} C_n, \qquad m = 1,2,\cdots,N_a \tag{I-3}$$

where β_{mn} is the so-called mutual impedance and it will be dealt with in Appendix II, and V_{im} is a function of the incident wave.

To account for the antenna copper loss, tangential E_t must be related to $\bar{J}$ by Ohm's law everywhere on the antenna. Let i,o,g denote the input, output, and ground terminals of the two-port, respectively. Then the first term of (I-3) reduces to (I-4) except for $m = i,o,g$ where additional terms due to the two-port must be considered.

$$\int_{L_m} ds\, f_m(\bar{r})\,\hat{u}_m \cdot \bar{E}_t(\bar{r}) = C_m \frac{kL_m - \sin(kL_m)}{2(1+\delta)k} \cdot \frac{2.61 \times 10^{-7} f^{1/2}}{\pi D_m} = C_m T_m \tag{I-4}$$

where f is the frequency and D_m the wire diameter. If we further assume that the physical dimensions of the input and output ports of the two-port are infinitesimal, then the following relations hold at the two-port

$$C_g f_g(0) = C_i f_i(0) - C_o f_o(0) \tag{I-5}$$

$$\int_{-\epsilon}^{0} \bar{E}_t \cdot \overline{ds}_i + \int_{0}^{+\epsilon} \bar{E}_t \cdot \overline{ds}_g = V_i \tag{I-6}$$

$$\int_{0}^{+\epsilon} \bar{E}_t \cdot \overline{ds}_g - \int_{0}^{+\epsilon} \bar{E}_t \cdot \overline{ds}_o = V_o. \tag{I-7}$$

For brevity, the argument of $f_i(0)$, $f_o(0)$, and $f_g(0)$ will henceforth be dropped. At the two-port, the voltages and currents are also governed by

$$\bar{V} = \bar{\bar{Z}} \cdot \bar{I} + \bar{\bar{U}} \cdot \bar{n}. \tag{I-8}$$

Form (I-3) and (I-5) through (I-8), the terminal voltages V_i and V_o and the constant C_g can be eliminated. The stage has now been set to calculate either the output signal or the output noise. To obtain the output signal, we remove all the noise generators, which is equivalent to setting $U_{ij} = U_{oj} = 0$ for all j in (I-8). The

resulting set of linear equations can be cast into the form

$$\bar{\nu} = \bar{\bar{\gamma}} \cdot \bar{C} \tag{I-9}$$

where the elements of $\bar{\bar{\gamma}}$ are given by

$$\gamma_{mn} = \beta_{mn}, \qquad \text{for} \quad \begin{cases} m \neq i,o,g \\ n \neq i,o,g \end{cases} \tag{I-10}$$

$$\gamma_{in} = \beta_{in} f_g + \beta_{gn} f_i, \qquad \text{for } n \neq i,o,g \tag{I-11}$$

$$\gamma_{on} = \beta_{on} f_g - \beta_{gn} f_o, \qquad \text{for } n \neq i,o,g \tag{I-12}$$

$$\gamma_{ii} = f_g\left(\beta_{ii} + \beta_{ig}\frac{f_i}{f_g}\right) + f_i\left(\beta_{gi} + \beta_{gg}\frac{f_i}{f_g}\right) - f_i^2 f_g Z_{ii} \tag{I-13}$$

$$\gamma_{io} = f_g\left(\beta_{io} - \beta_{ig}\frac{f_o}{f_g}\right) + f_i\left(\beta_{go} - \beta_{gg}\frac{f_o}{f_g}\right) - f_i f_g f_o Z_{io} \tag{I-14}$$

$$\gamma_{oi} = f_g\left(\beta_{oi} + \beta_{0g}\frac{f_i}{f_g}\right) - f_o\left(\beta_{gi} + \beta_{gg}\frac{f_i}{f_g}\right) + f_o f_g f_i Z_{oi} \tag{I-15}$$

$$\gamma_{oo} = f_g\left(\beta_{oo} - \beta_{og}\frac{f_o}{f_g}\right) - f_o\left(\beta_{go} - \beta_{gg}\frac{f_o}{f_g}\right) + f_o^2 f_g Z_{oo} \tag{I-16}$$

with $\beta_{ij} = \beta_{ij}' - T_i\delta_{ij}$, δ_{ij} being the Dirac delta function, and the elements of $\bar{\nu}$ are given by

$$\nu_i = -V_{ii} f_g - V_{ig} f_i \tag{I-17}$$

$$\nu_o = -V_{io} f_g + V_{ig} f_o \tag{I-18}$$

$$\nu_m = -V_{im}, \qquad \text{for } m \neq i,o,g. \tag{I-19}$$

The two-port terminal currents $f_i C_i$ and $f_o C_o$ can now be obtained by matrix inversion.

To obtain the output noise, we remove the incident field, which is equivalent to setting $V_{ij} = 0$, for all j in (I-3). The new set of linear equations is now in the form

$$\bar{\eta} = \bar{\bar{\gamma}} \cdot \bar{C} \tag{I-20}$$

where the elements of $\bar{\bar{\gamma}}$ are given by (I-10) through (I-16), and the elements of $\bar{\eta}$ are given by

$$\eta_i = f_i f_g \sum_{j=1}^{N} U_{ij} n_j \tag{I-21}$$

$$\eta_o = -f_o f_g \sum_{j=1}^{N} U_{oj} n_j \tag{I-22}$$

$$\eta_n = 0, \qquad \text{for } n \neq i,o,g. \tag{I-23}$$

From (I-20), the constants C_i and C_o can be obtained and the two-port terminal currents can be cast in the form

$$\bar{I} = \bar{\bar{\alpha}} \cdot \bar{\bar{U}} \cdot \bar{n} \tag{I-24}$$

where

$$\bar{\bar{\alpha}} = \begin{bmatrix} f_i^2 f_g (\bar{\bar{\gamma}}^{-1})_{ii}, & -f_i f_o f_g (\bar{\bar{\gamma}}^{-1})_{io} \\ f_i f_o f_g (\bar{\bar{\gamma}}^{-1})_{oi}, & -f_o^2 f_g (\bar{\bar{\gamma}}^{-1})_{oo} \end{bmatrix}. \tag{I-25}$$

Substitution of (I-24) into (I-8) yields

$$\bar{V} = \bar{\bar{Z}} \cdot \bar{\bar{\alpha}} \cdot \bar{\bar{U}} \cdot \bar{n} + \bar{\bar{U}} \cdot \bar{n} \tag{I-26}$$

which is (7) in the text.

APPENDIX II

EVALUATION OF MUTUAL IMPEDANCE

The junction of two or more straight segments can be thought of as the intersection of two or more half-dipoles of unequal lengths and magnitudes with the "centers" of the half dipoles superimposed on one another. Kirchhoff's current law is only invoked at the two-port junction. We, therefore, need to obtain the mutual impedance between two full dipoles, between a full dipole and a half-dipole, and between two half-dipoles. The general expression for the mutual impedance between two dipole elements is given by

$$\beta_{mn}' = \int ds \int ds'\, \hat{u}_m \cdot \bar{\bar{\Gamma}} \cdot \hat{u}_n \sin k\left(\frac{L_m}{2} - |s|\right) \sin k\left(\frac{L_n}{2} - |s'|\right) \tag{II-1}$$

where $\bar{\bar{\Gamma}}$ is the free-space tensor Green's function.

We shall evaluate the integral in (II-1) involving the primed coordinates first. Let the integral be denoted by $\bar{E}_{mn}$:

$$\bar{E}_{mn} = \int ds'\, \bar{\bar{\Gamma}} \cdot \hat{u}_n \sin k\left(\frac{L_n}{2} - |s'|\right) \tag{II-2}$$

which can be cast in the form

$$\bar{E}_{mn} = \hat{u}_z E_z + \hat{u}_\rho E_\rho \tag{II-3}$$

where

$$E_z{}^{\pm} = \frac{1}{j\omega\epsilon_0}\int \frac{\partial}{\partial z'}\left(-G\frac{f_n{}^{\pm}}{\partial z'} + f_n{}^{\pm}\frac{\partial G}{\partial z'}\right) dz' \tag{II-4}$$

$$E_p{}^{\pm} = \frac{1}{j\omega\epsilon_0}\int \frac{\partial^2 G}{\partial z \partial \rho} f_n{}^{\pm}\, dz' \tag{II-5}$$

with

$$f_n{}^{\pm} = \sin k\left(\frac{L_n}{2} \mp |s'|\right). \tag{II-6}$$

The positive and negative signs denote, respectively, the upper and lower half-dipoles. Evaluation of (II-4) is straightforward, and evaluation of (II-5) requires an artifice given in Jordan [8]. The results of the integration are

$$E_z{}^{+} = \frac{k}{4\pi j\omega\epsilon_0}\left\{\frac{\exp(-ikR_1)}{R_1} - \frac{\exp(-ikR_0)}{R_0}\left[\cos\frac{kL_n}{2} + jz\left(1 - \frac{j}{kR_0}\right)\sin\frac{kL_n}{2}\right]\right\} \tag{II-7}$$

$$E_z{}^{-} = \frac{k}{4\pi j\omega\epsilon_0}\left\{\frac{\exp(-ikR_2)}{R_2} - \frac{\exp(-ikR_0)}{R_0}\left[\cos\frac{kL_n}{2} - jz\left(1 - \frac{j}{kR_0}\right)\sin\frac{kL_n}{2}\right]\right\} \tag{II-8}$$

$$E_p{}^{+} = -\frac{k}{4\pi j\omega\epsilon_0 y}\left\{\frac{z - L_n/2}{R_1}\exp(-ikR_1) - \frac{\exp(-ikR_0)}{R_0}\cdot\left[Z\cos\frac{kL_n}{2} + \left(j\frac{z^2}{R_0} - \frac{1}{k} + \frac{z^2}{kR_0^2}\right)\right]\sin\frac{kL_n}{2}\right\} \tag{II-9}$$

$$E_p{}^{-} = -\frac{k}{4\pi j\omega\epsilon_0 y}\left\{\frac{z + L_n/2}{R_2}\exp(-ikR_0) - \frac{\exp(-jkR_0)}{R_0}\cdot\left[Z\cos\frac{kL_n}{2} - \left(j\frac{z^2}{R_0} - \frac{1}{k} + \frac{z^2}{kR_0^2}\right)\right]\sin\frac{kL_n}{2}\right\} \tag{II-10}$$

where R_0, R_1, R_2, y, and z are defined in Fig. 10 in which the centers of the two dipoles are coplanar with the yz plane.

REFERENCES

[1] H. H. Meinke, "Transistorized receiver antennas," Progress Rep. 6, Contract HF61(052)-950, Nov. 1967.

[2] ——, "Receiving antennas integrated with transistors," Progress Rep. 4, Contract F61052-69-C-0027, pp. 27–28, Nov. 1969.

[3] ——, "Research on antennas," Final Sci. Rep., Contract F61052-69-C-0027, Dec. 1, 1968 to Nov. 30, 1971.

[4] A. Van der Ziel, "Noise in junction transistors," *Proc. IRE*, pp. 1019–1038, June 1958.

[5] W. Guggenbuehl and M. J. O. Stratt, "Theory and experiments on shot noise in semiconductor junction diodes and transistors," *Proc. IRE*, pp. 839–854, June 1957.

[6] R. F. Harrington, "Matrix methods for field problems," *Proc. IEEE*, vol. 55, pp. 136–149, Feb. 1967.

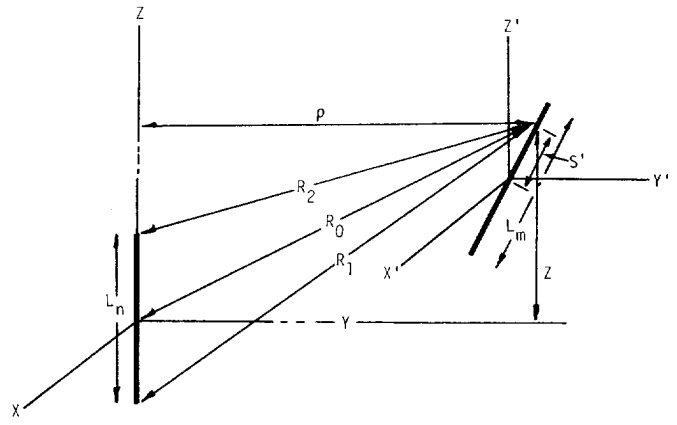

Fig. 10. Coordinate systems used to calculate field at any point on surface of mth dipole due to sinusoidal current on nth dipole.

[7] ——, *Field Computation by Moment Methods*. New York: Macmillan, 1968.
[8] E. C. Jordan, *Electromagnetic Waves and Radiating Systems*. Englewood Cliffs, N. J.: Prentice-Hall, 1950, pp. 342–369.
[9] G. J. Policky and H. F. Cooke, "The noise figure of microwave transistors," presented at Northeast Electron. Res. Eng. Meeting, Boston, Mass., Nov. 5, 1965.
[10] W. C. Wong, "Theoretical analysis of solid state antennas for direction finding," TRW Systems, under Air Force Contract F33615-71-C-1285, Air Force Avionics Lab., Air Force Systems Command, Wright-Patterson AFB, Ohio.

Three-Dimensional Corner Reflector Antenna

NAOKI INAGAKI

***Abstract*—A reflector antenna utilizing three planar reflectors and a 3/4 λ-unipole radiator is proposed. Calculations based on image- and EMF-methods predict that the gain is about 5 dB greater than that of the two-dimensional corner reflector antenna, and that the input impedance is roughly between 50 and 75 Ω. Experiments conducted on the three-dimensional corner reflector antenna with rectangular corners confirmed the predicted properties and also showed the sidelobe in the electric plane being suppressed by the effect of diffraction. This effect is explained by the calculated radiation pattern of 3/4 λ-unipole on conducting half plate.**

PRINCIPLE OF THE ANTENNA

The antenna consists of three planar reflectors and a 3/4 λ-unipole (λ is wavelength) located on one of the reflectors, as shown in Fig. 1. If the ground plane dimension l is infinitely large, the radiation pattern is exactly that of a 3/2 λ-dipole inside the corner reflector, which becomes maximum at $\theta = \theta_0 \simeq \pi/4$ and $\phi = \alpha/2$, by choosing the corner angle α and the distance d between the apex and the unipole properly. The sidelobe at $\theta \simeq \pi/2$ will be suppressed if the ground plane dimension l is finite.

ANALYSIS BY IMAGE- AND EMF-METHOD

Assuming a sinusoidal current for the unipole and infinite dimensions for the reflectors, we get the following far field when $\alpha = \pi/n$ (n is an arbitrary integer):

$$E_\theta = j\frac{\exp(-jkr)}{2\pi r}\eta I_0 \frac{\cos(\frac{3}{2}\pi\cos\theta)}{\sin\theta} A(\theta,\phi), \qquad k = \omega(\mu_0\epsilon_0)^{1/2}$$

$$\eta = (\mu_0/\epsilon_0)^{1/2} \quad (1)$$

where I_0 is the input current, (r,θ,ϕ) is the spherical coordinate, and $A(\theta,\phi)$ is the array factor of the ring array consisting of the radiator and the images [1] whose functional forms in both E- and quasi-H-planes are given in Table I. The quasi-H-plane is defined as the plane intersecting perpendicularly the E-plane through the direction of maximum radiation $(\theta_0,\alpha/2)$ as shown in Fig. 1. The new variable ψ is introduced as the deviating angle from $(\theta_0,\alpha/2)$ in the quasi-H-plane, which is related to θ by

$$\cos\theta_0 \cos\psi = \cos\theta. \quad (2)$$

It has been found from (1) that θ_0 decreases linearly from about 50° to 30°, as d/λ increases from 0.5 to 1.2, for $\alpha = 90°$, from 0.7 to 1.4, for $\alpha = 60°$, and from 1.0 to 1.8, for $\alpha = 45°$. It has been also recognized that the half power beamwidths in both the E- and the quasi-H-planes are almost the same.

Fig. 2 shows the calculated and measured radiation patterns for $\alpha = 90°$. Three reflectors of the constructed antenna are cut square with $l = 2\lambda$. It is seen that the sidelobe at $\theta \simeq \pi/2$ appearing in the calculated patterns is extremely suppressed in the measured ones.

The input impedance $Z_{in} = R + jX$ was calculated from the self- and mutual-impedances of the radiators and the images based on the EMF method, and is plotted against d in Fig. 3 with α as a parameter. The resistance is roughly between 50 and 75 Ω for proper radiator location, while the reactance is as low as 10 Ω, which suggests that the direct feed by coaxial cables is possible. In the same figure, the measured input impedance for the antenna with $\alpha = 90°$ and $l = 2\lambda$ is included. Both the measured R and X show similar dependence on d as the calculated ones, although the measured X are smaller and are practically welcome.

Once the input resistance is known, the gain G of the antenna may be calculated by the formula

$$G(\theta,\phi) = \frac{4\pi r^2(1/\eta)\,|E_\theta|^2}{RI_0^2} = \frac{\eta}{\pi R}\frac{\cos^2(\frac{3}{2}\pi\cos\theta)}{\sin^2\theta}\,|A(\theta,\phi)|^2. \quad (3)$$

The gain in the directions $(\theta = \pi/4, \phi = \alpha/2)$ and $(\theta = \theta_0, \phi = \alpha/2)$ are plotted in Fig. 4 against d with α as a parameter. The maximum obtainable gain exceeds that of the conventional two-dimensional corner reflector antenna by about 5 dB in every case. The optimum value of $d/\lambda(d_{op}/\lambda)$ is 0.9, for $\alpha = 90°$, 1.2, for $\alpha = 60°$, and 1.6, for $\alpha = 45°$.

Manuscript received July 10, 1963; revised January 21, 1974.
The author is with the Department of Electronics, Nagoya Institute of Technology, Nagoya, Japan.

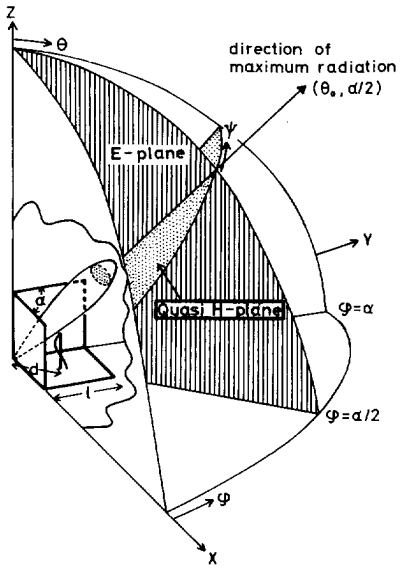

Fig. 1. Geometry of three-dimensional corner reflector antenna.